Supplementary Materials for

Upper crustal accretion by melt sill and lava flow interaction

This file includes:

Supplementary Figures 1-20

Supplemental Movies 1-5

Supplemental Movie 1 | Inline profiles from 101 ~ 538.

Supplemental Movie 2 | Xline profiles from 1001 ~ 4200.

Supplemental Movie 3 | Three-dimensional rotating Fig.2 with lava flow base surface.

Supplemental Movie 4 | Three-dimensional rotating Fig.3 with lava flow base surface.

Supplemental Movie 5 | Three-dimensional rotating Extended Data Fig. 2 with lava flow base surface.

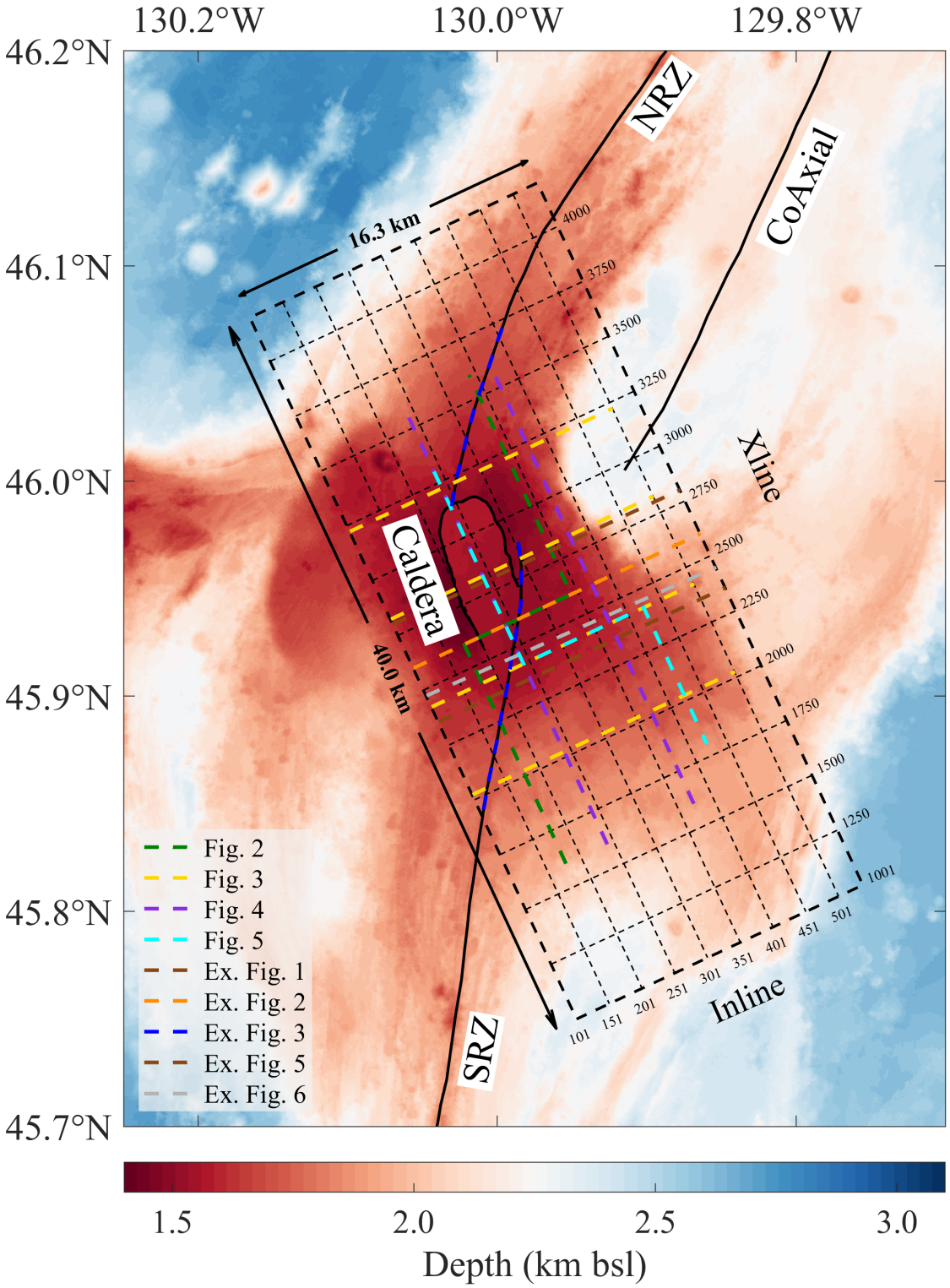

Supplementary Figure 1 | The locations of all profiles used in main text: A bathymetric map of the Axial volcano area, showing the north rift zone (NRZ), south rift zone (SRZ), and Co-Axial segment of the Juan de Ridge. The thick black dashed rectangle indicates the area of the 3D seismic reflection box and thin black dashed lines mark the Inline and Xline numbers. The dash colourful lines indicate the reflection profiles used in Figures and Extended Data Figures (legends inserted in the upper left corner).

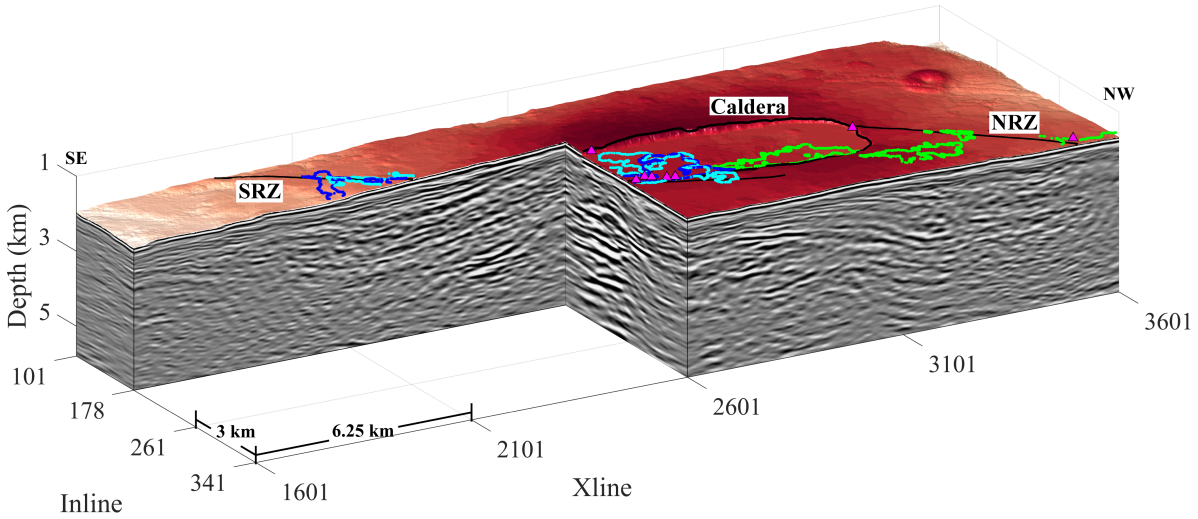

Supplementary Figure 2 | Lava flows (non-interpreted Fig. 2): A block diagram showing Inline (178 and 357) seismic reflection images crossing the south rift zone (SRZ) and north rift zone (NRZ). Locations of hydrothermal fields are shown as small, magenta-filled triangles[1]. Outlines of the 1998 (blue), 2011 (cyan) and 2015 (green) eruption lava flows are overlain on the bathymetric map[2–4].

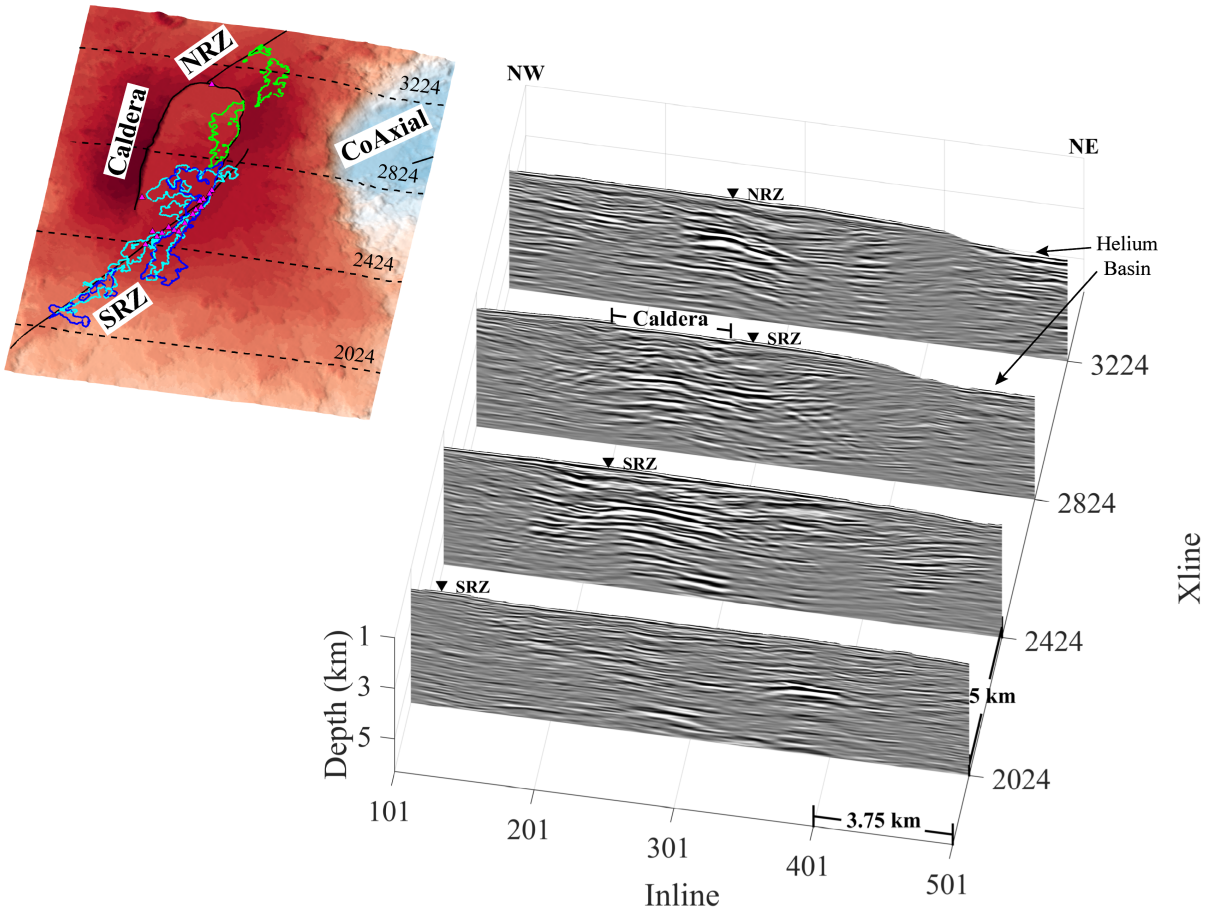

Supplementary Figure 3 | Xlines (non-interpreted Fig. 3): Four representative Xlines (5 km apart) showing lava flow layering, melt lenses and faults. NRZ: north rift zone, SRZ: south rift zone. The locations of the lines are shown on the map (left). Xlines 2024 and 2424 are southeast of the caldera, Xline 2824 crosses the caldera in the middle and Xline 3224 is northwest of the caldera. Locations of hydrothermal fields are shown as small, magenta-filled triangles[1]. Outlines of the 1998 (blue), 2011 (cyan) and 2015 (green) eruption lava flows are overlain on the bathymetric map[2–4].

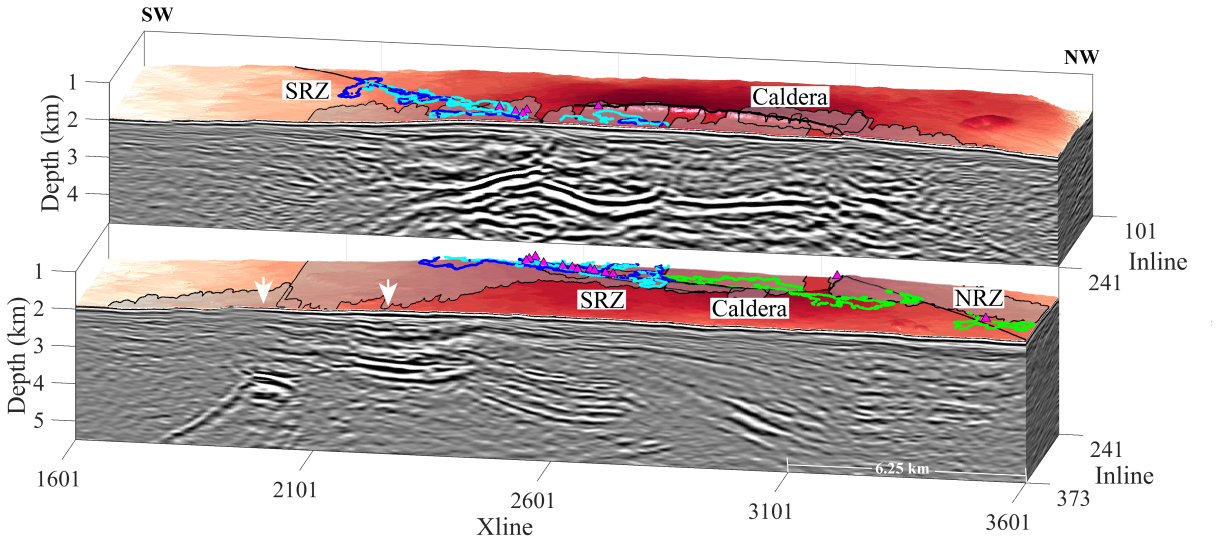

Supplementary Figure 4 | Lava flow–melt sill interaction (non-interpreted Fig. 4): Block diagram showing Inline (241 and 373) seismic reflection images. Inline profile 373, northeast of caldera, showing lava flow layers interacting with melt sills at five locations over 25 km along the profile. White arrows indicate the two melt sills reported by Kent et al. (2025)[5]. Inline 241 showing lava flow layering above melt body beneath the caldera. Locations of hydrothermal fields are shown as small, magenta-filled triangles[1]. Outlines of the 1998 (blue), 2011 (cyan) and 2015 (green) eruption lava flows are overlain on the bathymetric map[2–4].

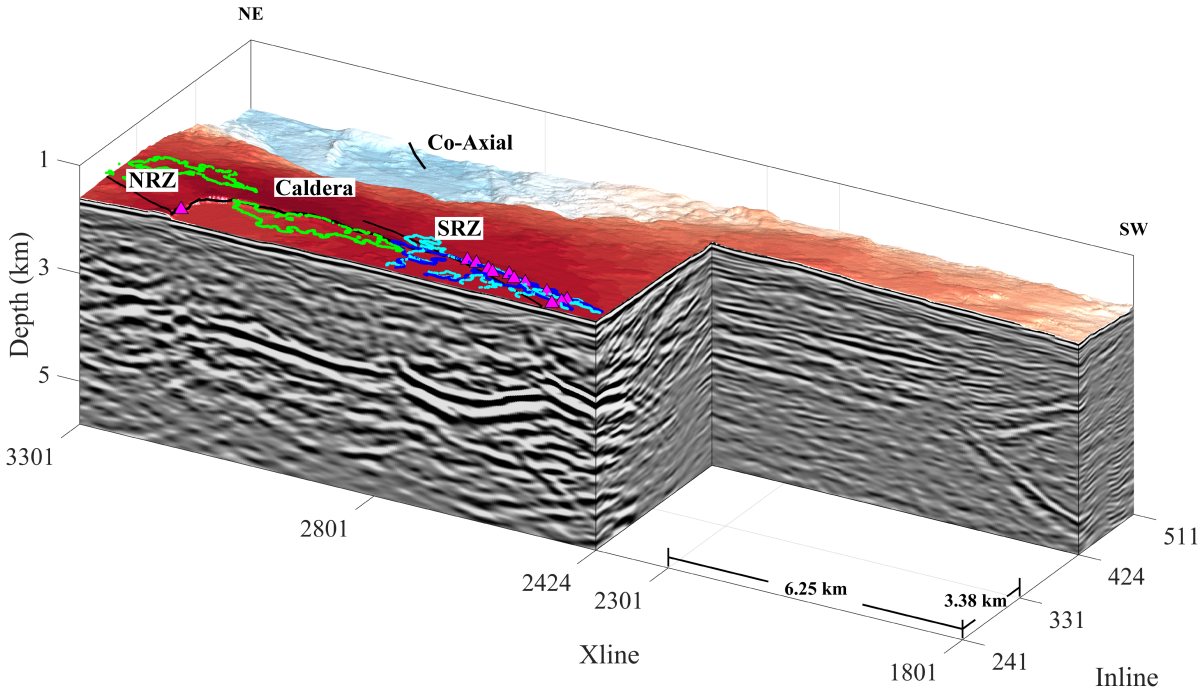

Supplementary Figure 5 | Melt sills injected along lava flows (non-interpreted Fig. 5): Block diagram showing Inline (241 and 424) and Xline (2424) seismic reflection images. Inline 241 showing lava stratigraphy and listric faults above melt body beneath the caldera. Inline 424 and Xline 2424 showing melt sills injected along lava flows. Locations of hydrothermal fields are shown as small, magenta-filled triangles[1]. Outlines of the 1998 (blue) and 2015 (green) eruption lava flows is overlain on the bathymetric map[2–4].

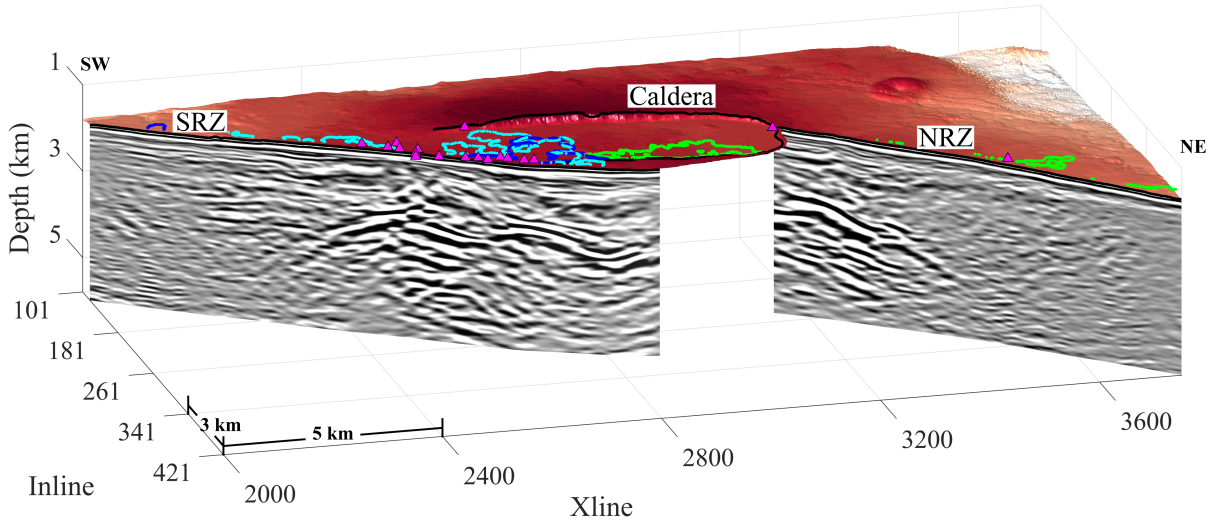

Supplementary Figure 6 | Seismic images along rift zones (non-interpreted Extended Data Fig. 2): Rift coincident seismic images along the north (NRZ) and south rift zones SRZ (light blue lines in Supplementary Fig. 1). Locations of hydrothermal fields are shown as small, magenta-filled triangles[1]. Outlines of the 1998 (blue), 2011 (cyan) and 2015 (green) eruption lava flows are overlain on the bathymetric map[2–4].

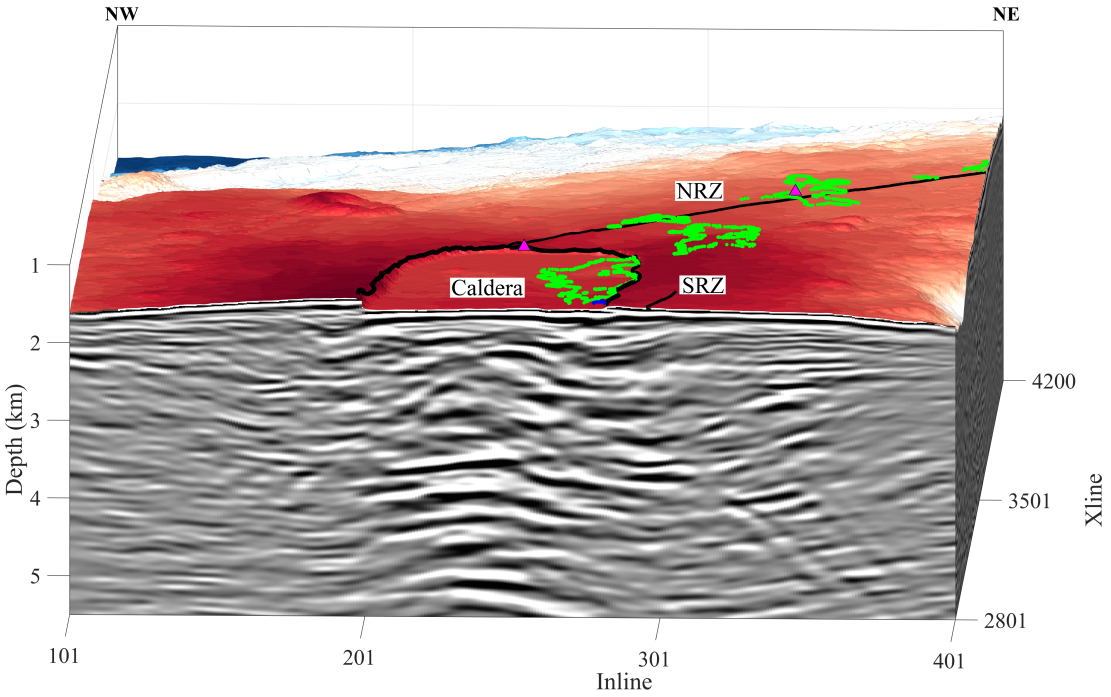

Supplementary Figure 7 | Seismic image along Xline profile 2801 (non-interpreted Extended Data Fig. 5): Seismic image showing inflation (convex) and deflation (concave) of melt sills leading to uplift and subsidence of lava flows beneath caldera. Note the merging of lava flows with melt sills around Inline 301 at ~3.5 km depth. Locations of hydrothermal fields are shown as small, magenta-filled triangles[1]. Outlines of the 1998 (blue) and 2015 (green) eruption lava flows is overlain on the bathymetric map[2–4].

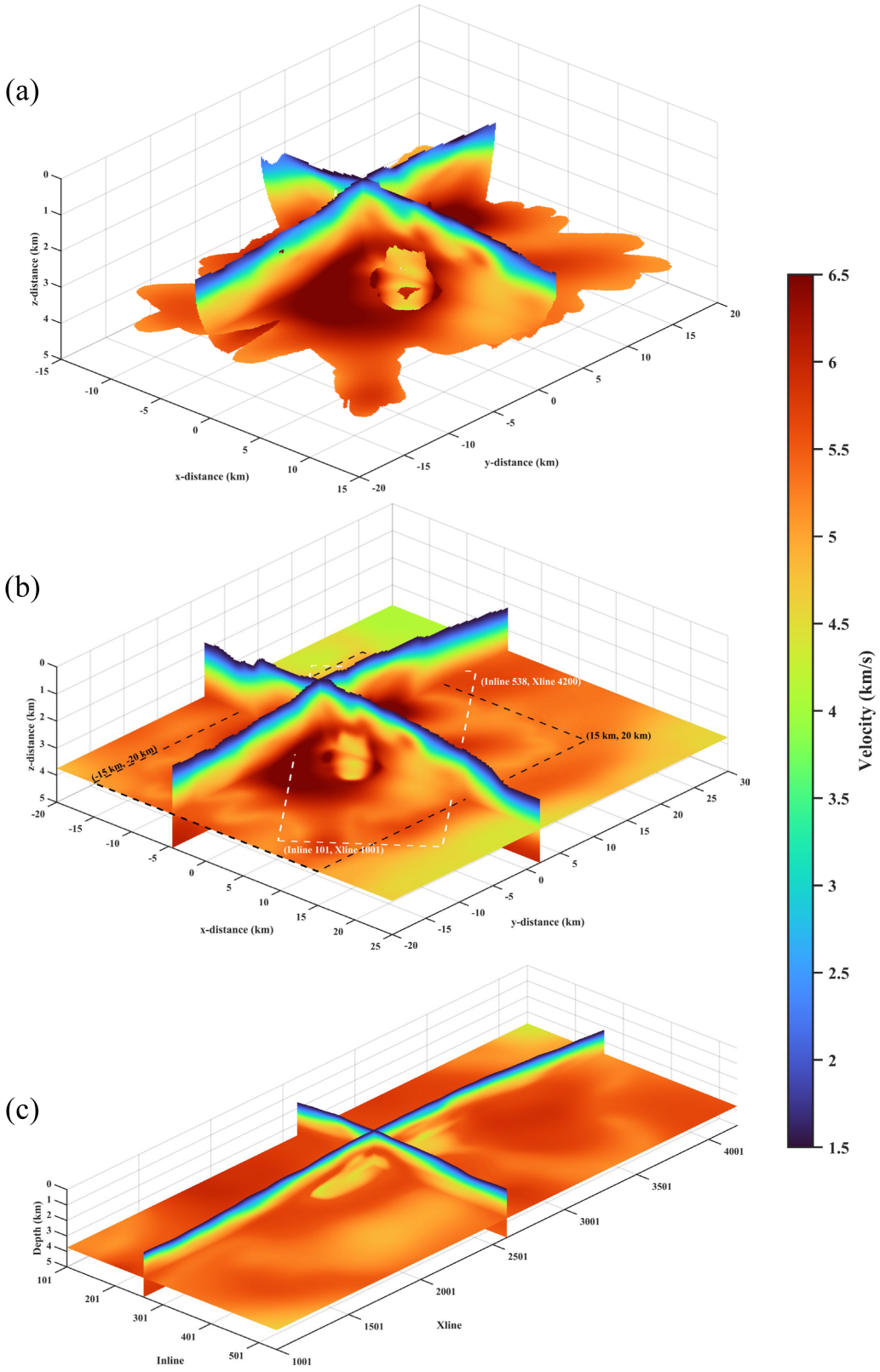

Supplementary Figure 8 | Construction of the initial velocity model: (a) The 3D tomographic velocity model from Arnulf et al. (2018)[6]. (b) The modified 3D velocity model after gap filling, 3D smoothing, water column velocity adjustment, and out-of-bounds velocity assignment. The black box outlines the original extent of the tomographic model, while the white box marks the survey area of this study. (c) The final 3D velocity model extracted and resampled within the study area.

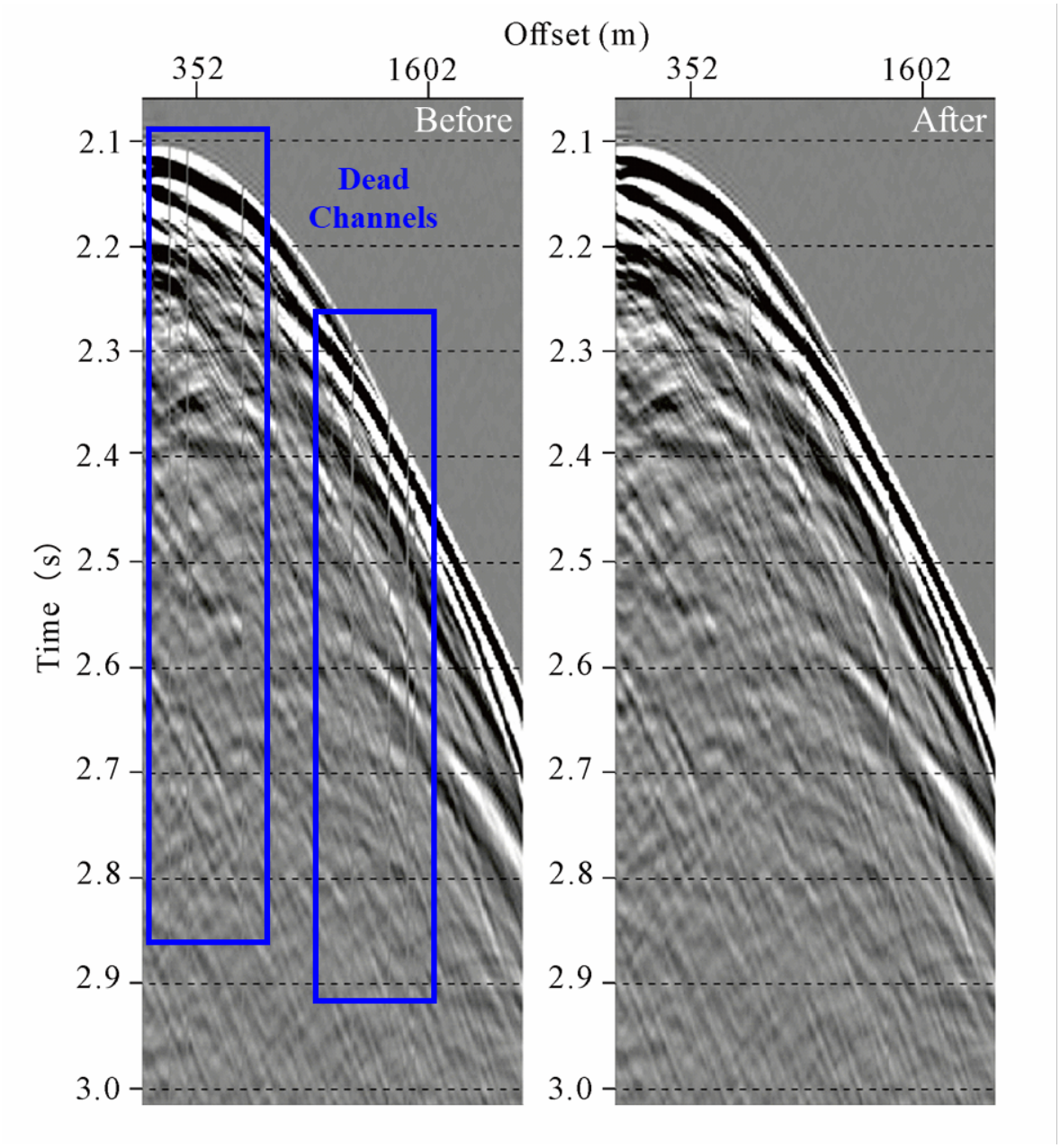

Supplementary Figure 9 | Interpolation: a shot gather before (left) and after (right) data interpolation. The blue boxes emphasize the dead channels.

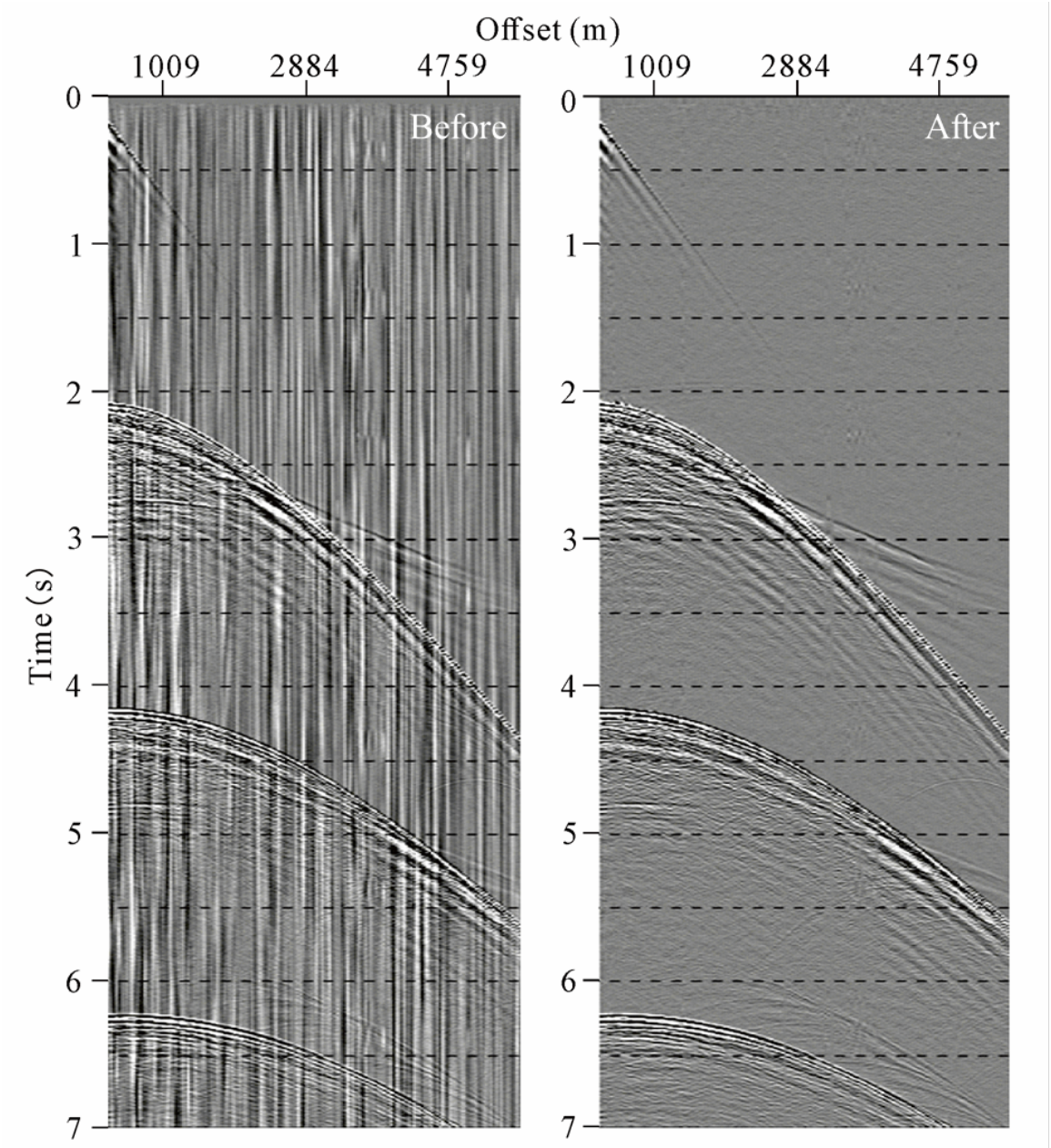

Supplementary Figure 10 | Swell noise attenuation: a shot gather before (left) and after (right) swell noise attenuation.

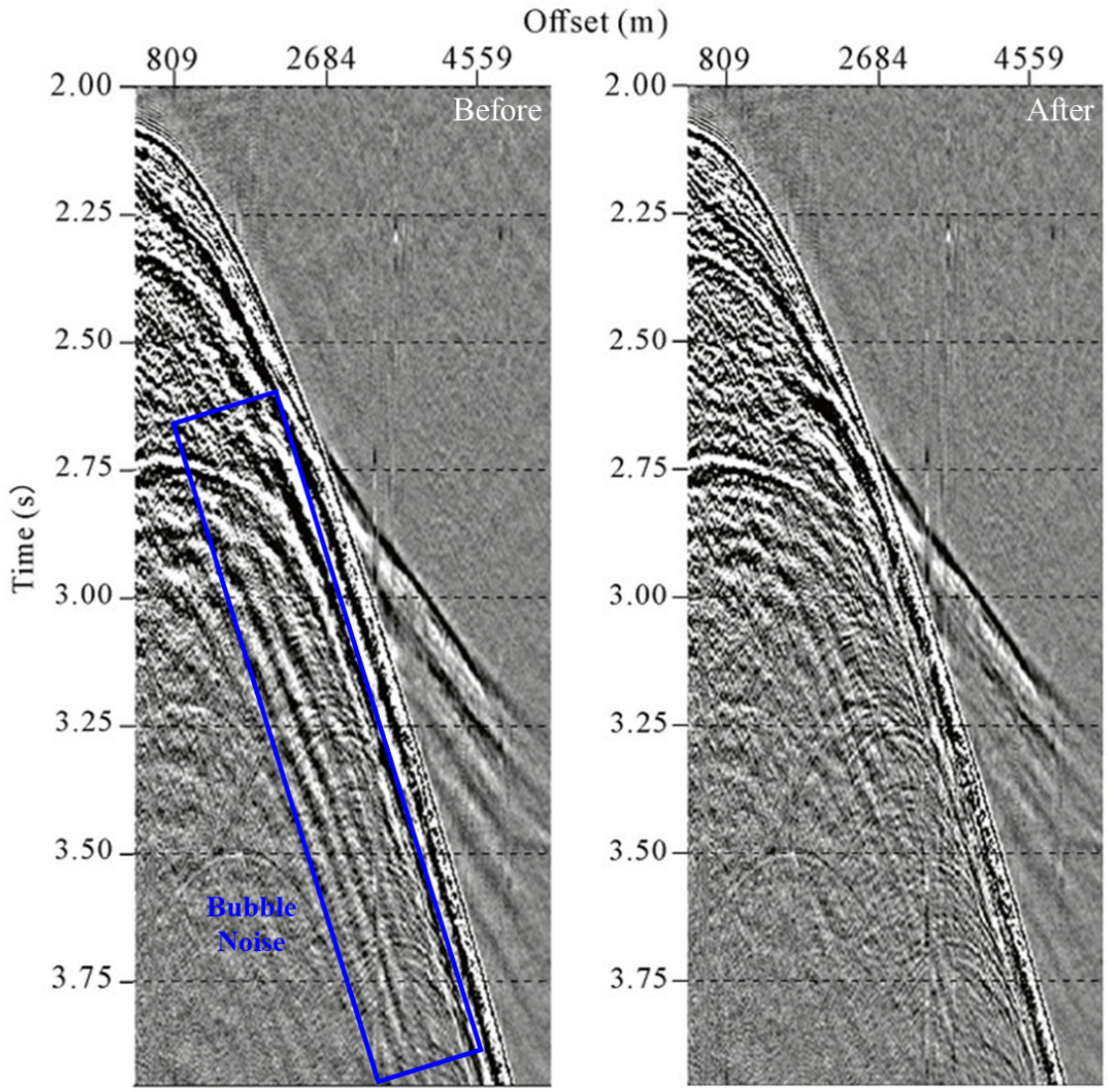

Supplementary Figure 11 | Deconvolution: a shot gather before (left) and after (right) deconvolution. The blue box emphasizes the bubble noise.

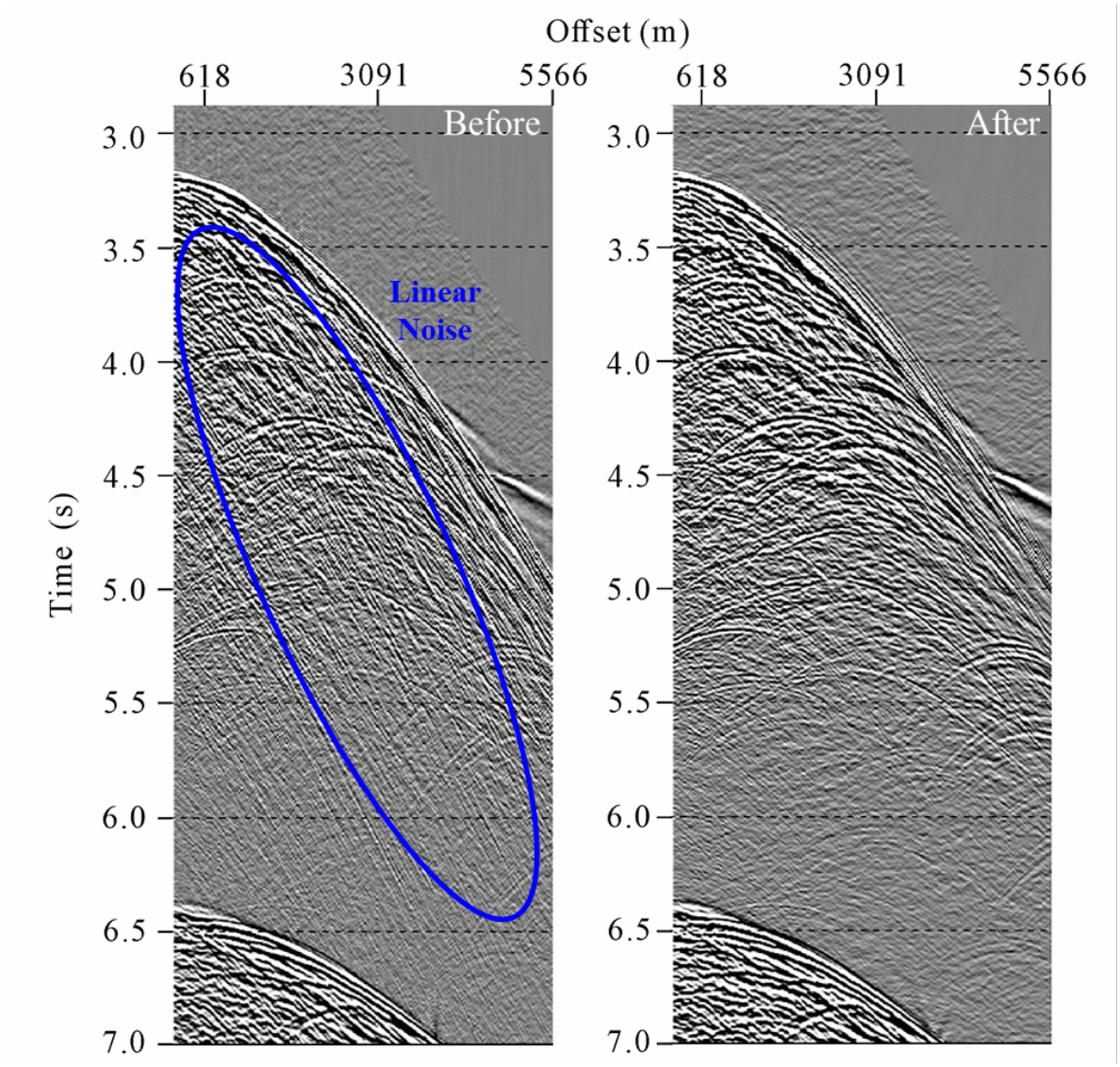

Supplementary Figure 12 | Linear dipping noise removal: a shot gather before (left) and after (right) linear dipping noise removal. The blue circle emphasizes the linear dipping noise.

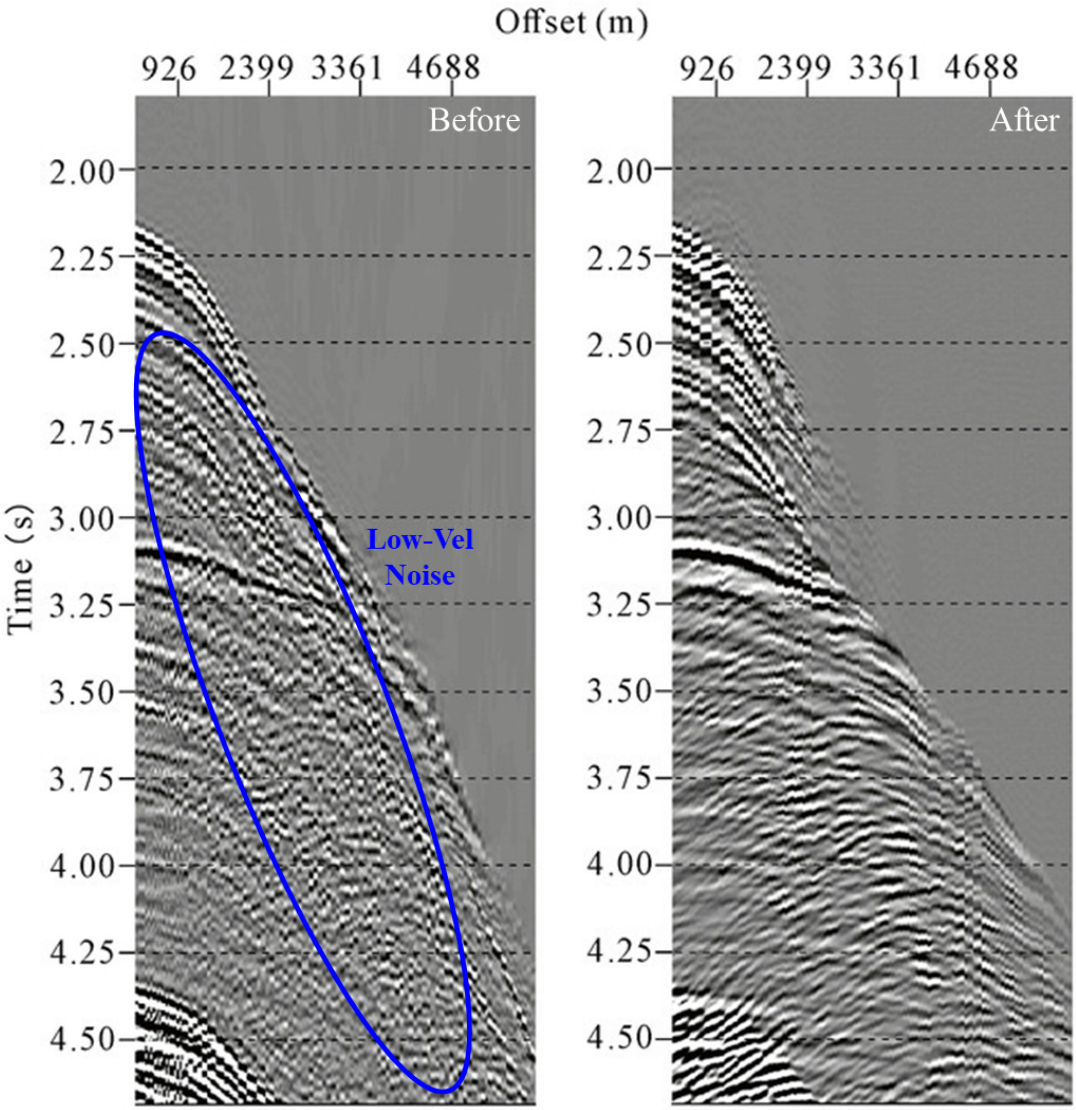

Supplementary Figure 13 | Low velocity energy suppression: a common-midpoint gather (CMP) gather before (left) and after (right) suppression of energy travelling with low-velocities. The blue circle emphasizes the low velocity noise.

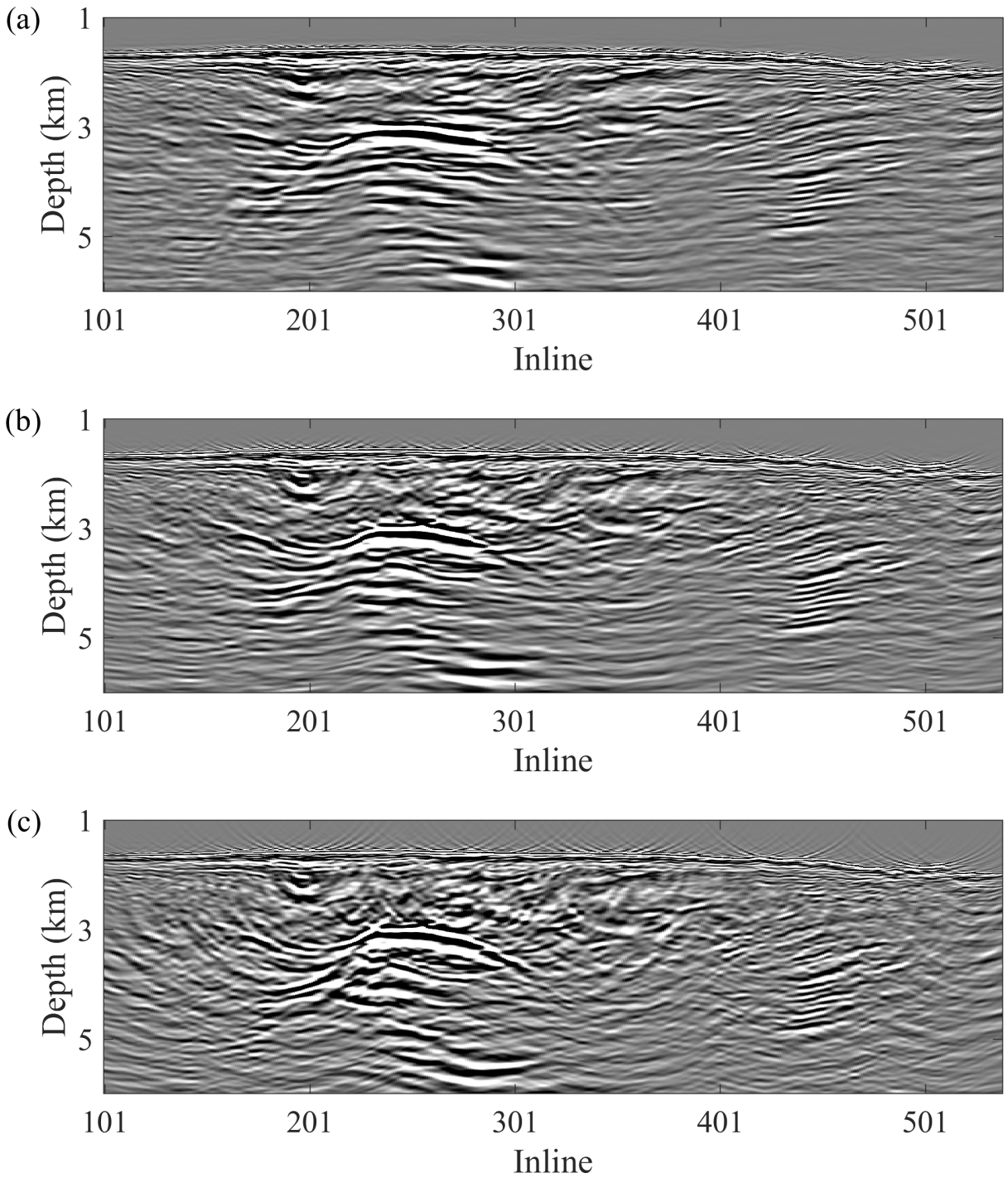

Supplementary Figure 14 | Comparison of Xline 2424 image using different migration apertures along Xline direction. (a) image using 1 km aperture, (b) image using 2 km aperture, (c) image using 4 km aperture. 4 km aperture does the best job of reconstructing dipping flanks of the magma domain, but at the expense of migration artifacts reducing clarity of the lava stratigraphy.

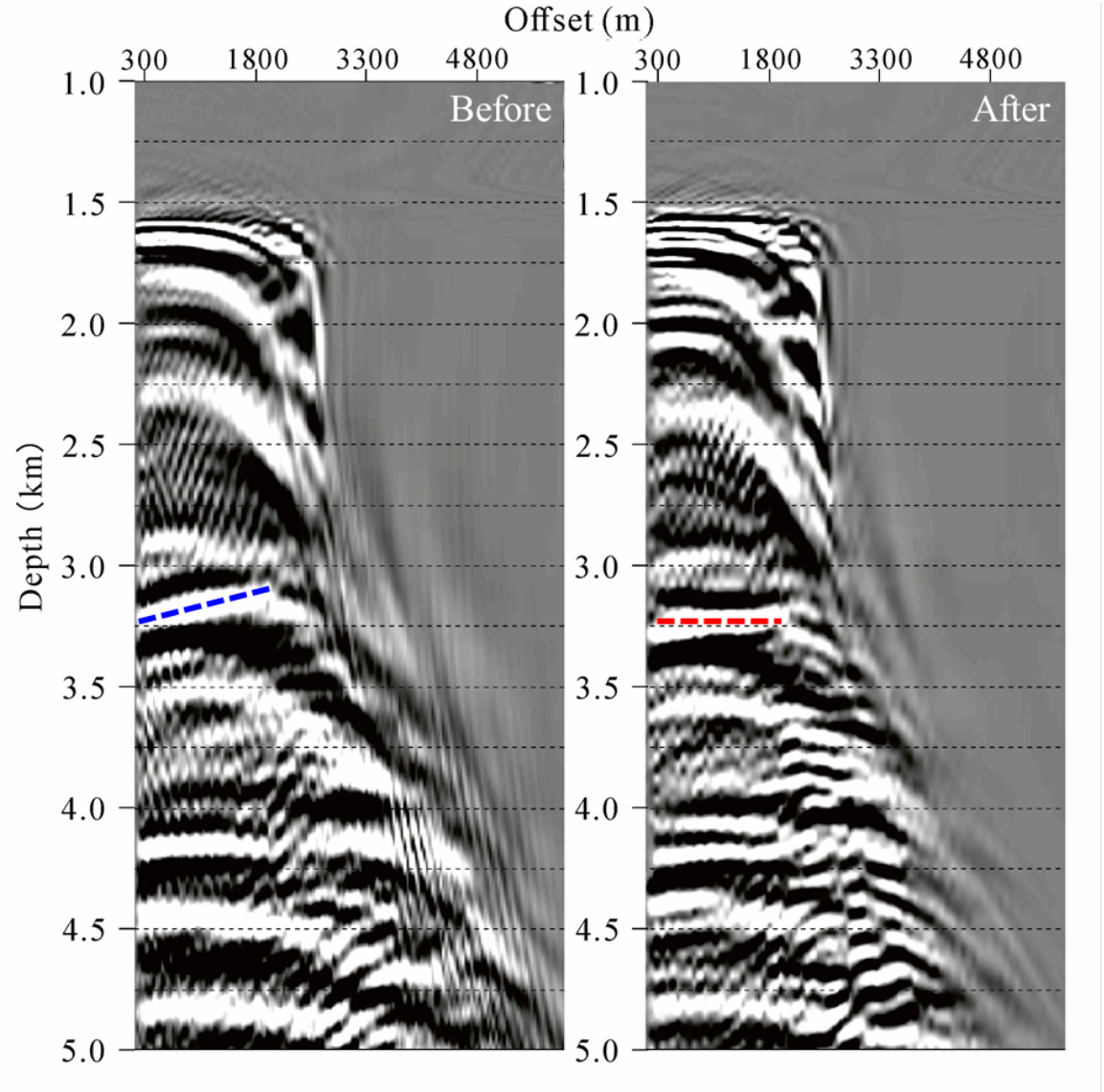

Supplementary Figure 15 | Residual Moveout (RMO) Correction: a common imaging gather (GIG) before (left) and after (right) the RMO correction. The blue and red dotted lines indicate the angle of the same event before and after the correction.

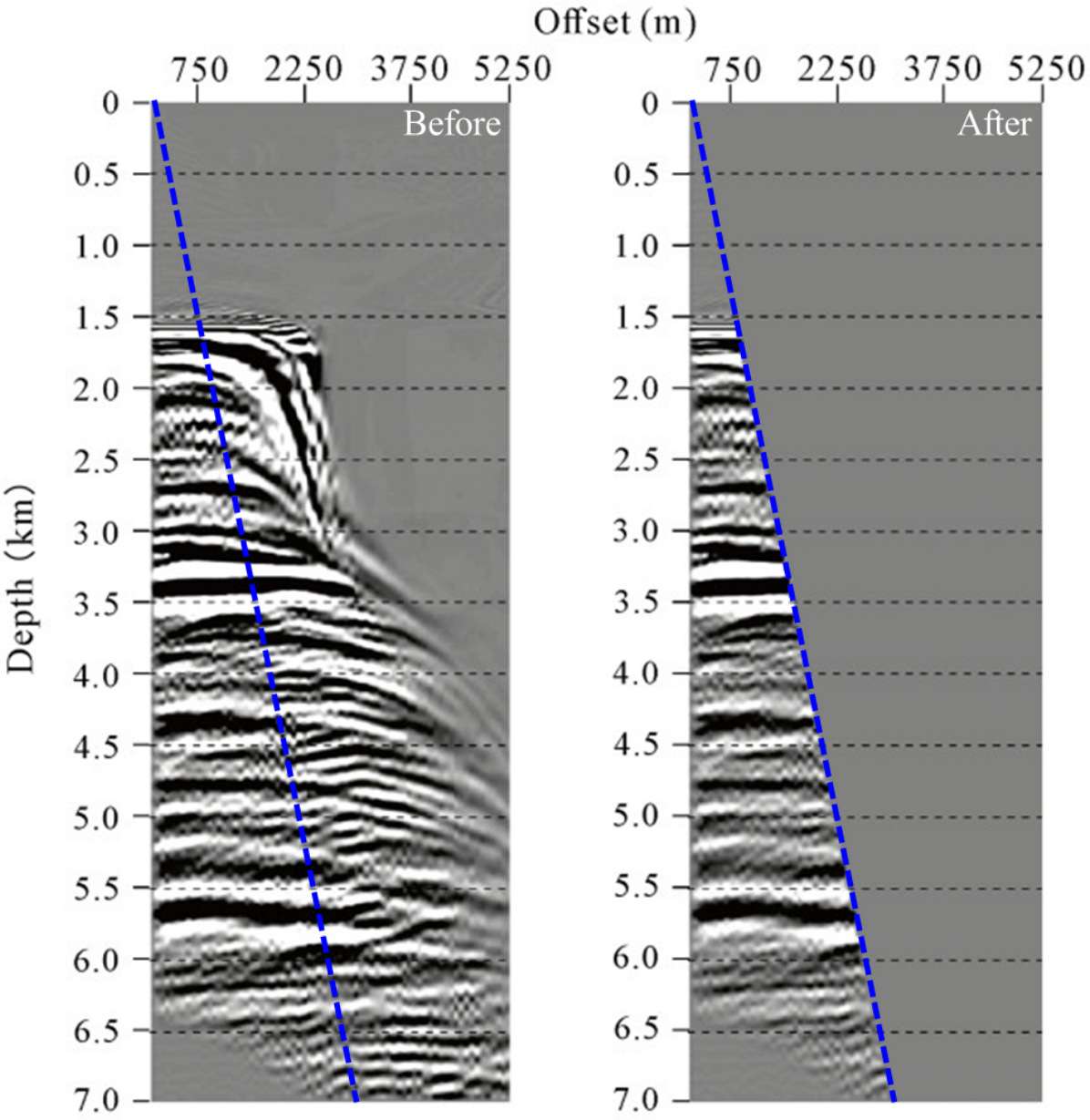

Supplementary Figure 16 | Common imaging gather (GIG) muting: a common imaging gather (GIG) before (left) and after (right) muting strategy. The blue dotted lines indicate the boundary of the muting function.

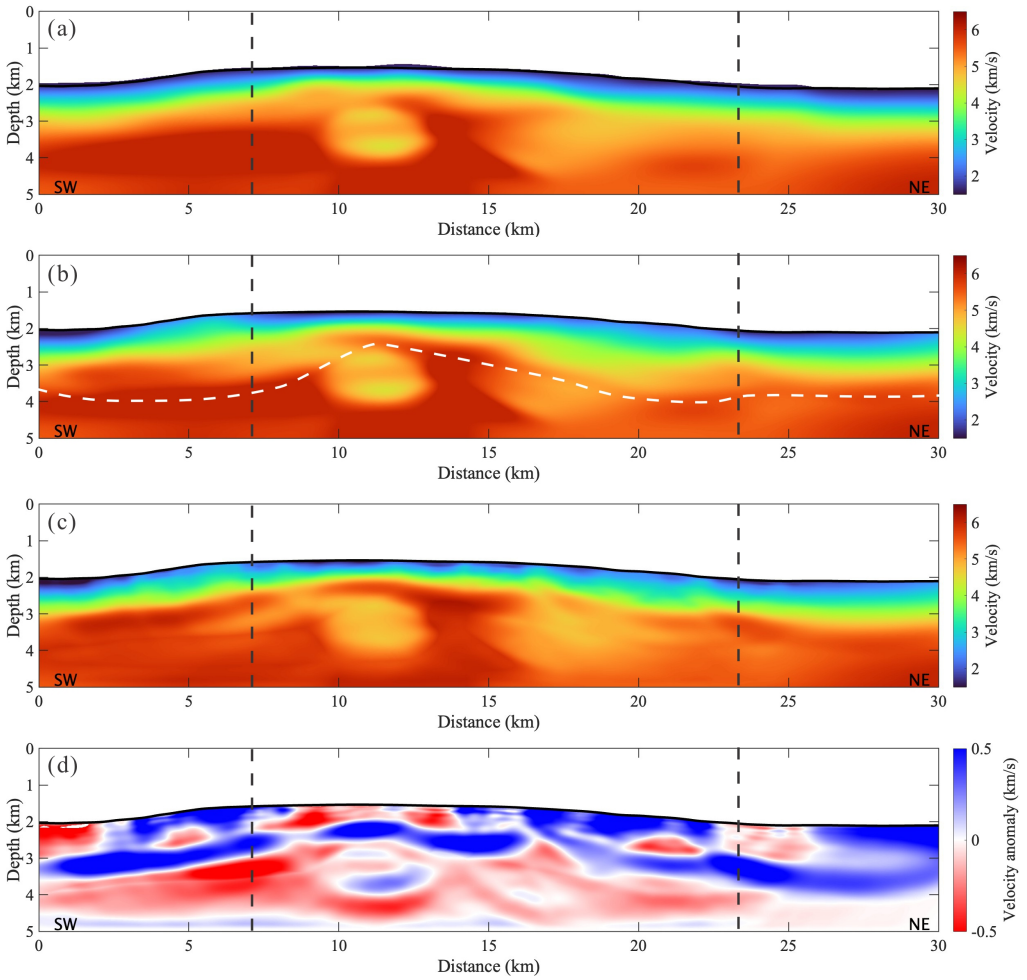

Supplementary Figure 17 | Velocity Models: (a) initial model for velocity inversions. (b) inverted model produced by travel time tomography, the white dash line indicates the maximum depth of ray coverage. (c) inverted model produced by FWI using the velocity in (b) as an initial model. (d) Velocity updates to the initial model after tomography and FWI. The black dashed lines indicate the range of velocity displays in Extended Data Fig. 7.

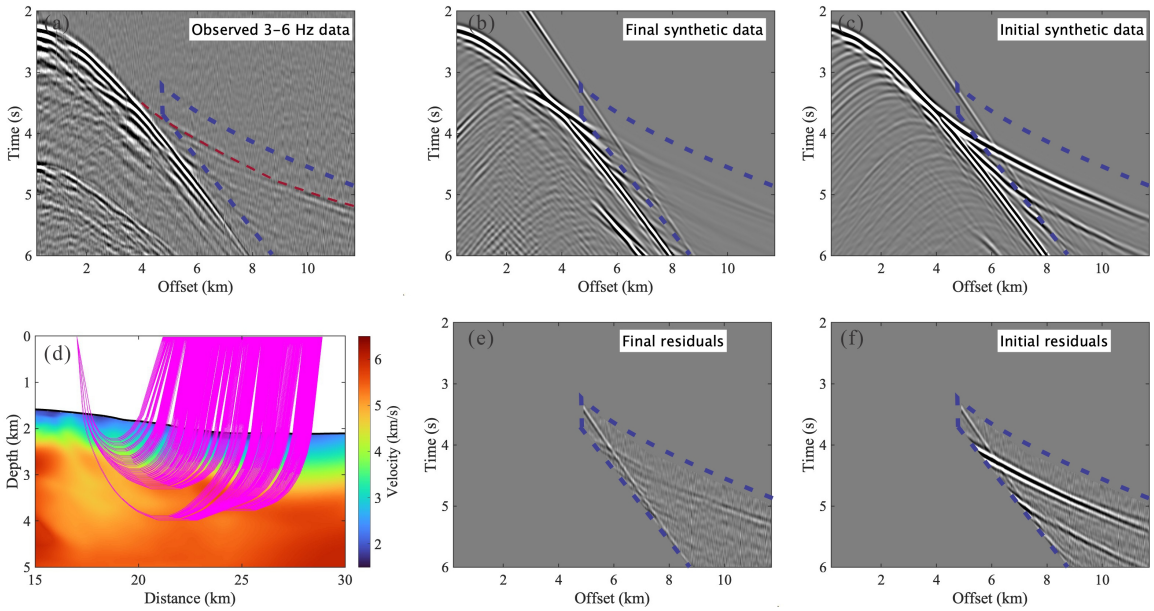

Supplementary Figure 18 | An Example of 2D MCS data waveforms and residuals. (a) Shot gather No. 1229 at 17 km distance along the profile. The red dashed line is the travel time picked from the wide-angle first arrivals for travel time tomography. (b) Synthetic data produced by final model of FWI. (c) Synthetic data produced by initial model of FWI (tomographic model). (d) The location of the shot gather and corresponding ray traces. (e) Data residual between final synthetic data and observed data. (f) Data residual between initial synthetic data and observed data. Blue lines indicate the mute window for FWI.

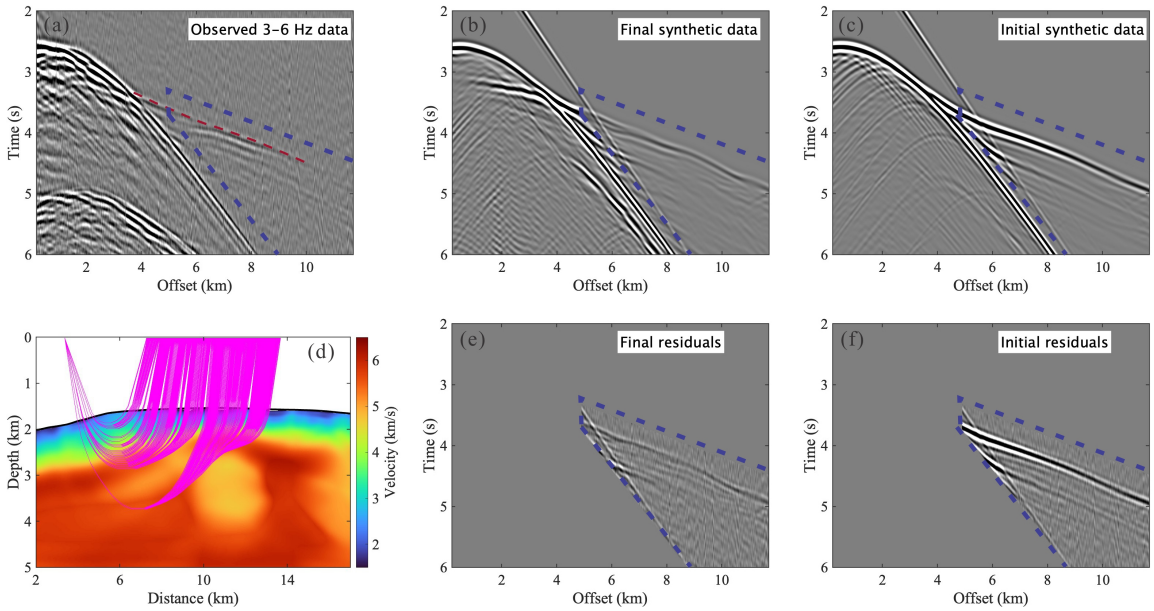

Supplementary Figure 19 | An Example of 2D MCS data waveforms and residuals. (a) Shot gather No. 1593 at 3 km distance along the profile. The red dashed line is the travel time picked from the wide-angle first arrivals for travel time tomography. (b) Synthetic data produced by final model of FWI. (c) Synthetic data produced by initial model of FWI (tomographic model). (d) The location of the shot gather and corresponding ray traces. (e) Data residual between final synthetic data and observed data. (f) Data residual between initial synthetic data and observed data. Blue lines indicate the mute window for FWI.

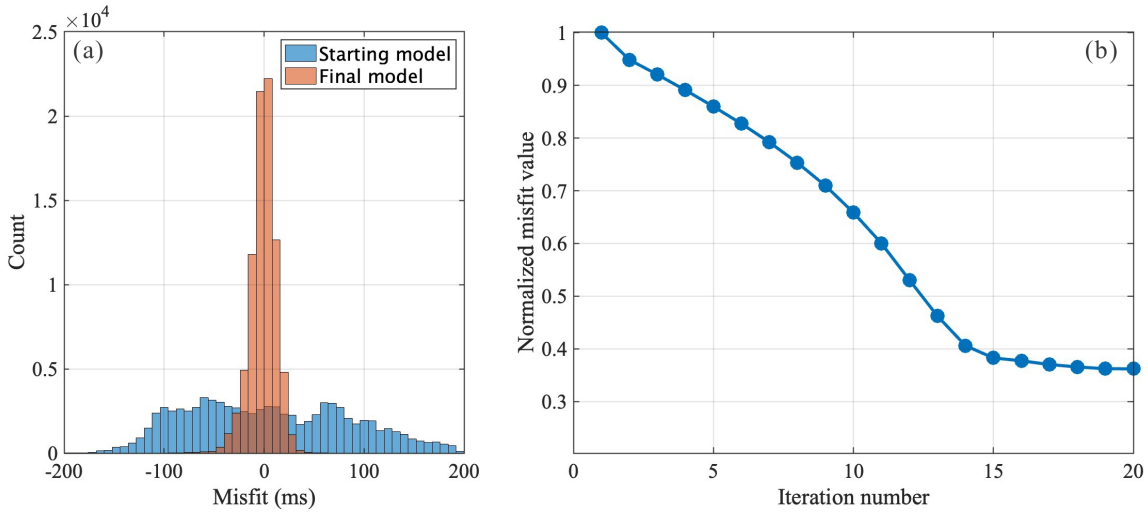

Supplementary Figure 20 | Misfit variation during velocity inversions. (a) Travel time residual histograms of the initial and final models involved in tomography. (b) Objective function misfit values of each FWI iteration.

Reference

1. Baker, E. T. *et al.* Posteruption Enhancement of Hydrothermal Activity: A 33-Year, Multieruption Time Series at Axial Seamount (Juan de Fuca Ridge). *Geochem. Geophys. Geosystems* **20**, 814–828 (2019).
2. Caress, D. *et al.* Interpreted outlines (version 1) as ASCII points of the 2011 lava flows and eruptive fissures at Axial Seamount, Juan de Fuca Ridge (investigator David Caress). Interdisciplinary Earth Data Alliance (IEDA) https://doi.org/10.1594/IEDA/323602 (2018).
3. Chadwick, W. *et al.* Interpreted outlines as ASCII points of the 1998 lava flows and eruptive fissures at Axial Seamount, Juan de Fuca Ridge (investigator William Chadwick). Interdisciplinary Earth Data Alliance (IEDA) https://doi.org/10.1594/IEDA/323601 (2018).
4. Clague, D. *et al.* Interpreted outlines (version 2) as shapefiles of the 2015 lava flows and eruptive fissures at Axial Seamount, Juan de Fuca Ridge (investigator David Clague). Interdisciplinary Earth Data Alliance (IEDA) https://doi.org/10.1594/IEDA/324417 (2018).
5. Kent, G. *et al.* Melt Focusing and Assimilation Along the Lithosphere-Asthenosphere Boundary Beneath Axial Volcano. *Nature* **Accepted**, (2025).
6. Arnulf, A. F., Harding, A. J., Kent, G. M. & Wilcock, W. S. D. Structure, Seismicity, and Accretionary Processes at the Hot Spot-Influenced Axial Seamount on the Juan de Fuca Ridge. *J. Geophys. Res. Solid Earth* **123**, 4618–4646 (2018).